Egypt. J. Phys. **Vol. 51,** pp. 101-114 (2023)

Egyptian Journal of Physics

https://ejphysics.journals.ekb.eg/

Characterization of Renal Stone Composition Using the Dual-Energy Technique of Computed Tomography: An in Vitro Study

Mohamed Z. El-Sayed, Mohamed M. El Safwany, Bothaina A. Kandil and Magdi A. Ali
Faculty of Applied Health Science Technology, Pharos University in Alexandria, Alexandria, Egypt.

The determination of the composition of different types of renal stones using dual energy computed tomography is essential for the selection of an appropriate management strategy. Examine the role of dual energy computed tomography in the in vitro characterization of renal stones and confirm the findings using an X-ray diffraction pattern and Fourier transform infrared spectroscopy. Included were forty randomly collected renal stones that underwent dual energy computed tomography for characterization of urinary calculi. insert stones in the bovine kidney model. Linear attenuation coefficients were measured. The dual energy ratio and index were calculated and used to detect the composition of renal stones. To establish the composition of renal stones, an X-ray diffraction pattern and Fourier transform infrared spectroscopy were used. Dual energy computed tomography can differentiate between uric acid (UA) and calcified stones. A dual energy ratio of 1.02 to 1.1 correctly predicted UA stones, while a ratio of 1.24 to 1.65 correctly predicted calcium-containing stones. A dual energy index between 0.00174 and 0.00918 accurately predicted UA stones, and a dual energy index between 0.0495-0.1497 accurately predicted calcium containing stones. Through the in-vitro study, dual energy computed tomography characterized 2/40 UA containing stones and characterized 38/40 calcium containing stones. The characterization of the dual-energy computed tomography renal stones proved to be extremely compatible with the X-ray diffraction pattern and Fourier transform infrared spectroscopy. This study demonstrates that dual-energy computed tomography can be employed in vitro to accurately differentiate between UA and calcified renal stones.
Keywords: DECT, Renal stones, Stone composition, UA, Calcium, in-vitro.

Introduction

Urolithiasis is one of the most common urinary system diseases. It is a global health issue, and its prevalence and incidence have been reported to be increasing over the last several decades, particularly in industrialized countries. It is thought to be a complex disease, including epidemiological, biochemical, and genetic variables.[1]

A stone's composition can be determined using a variety of techniques, including Fourier transform infrared spectroscopy (FTIR) and X-ray powder diffraction (XRD). These are used to analyse the composition of stones and identify the type and quantity. [2,3]

Medical imaging using computed tomography (CT) has lately advanced rapidly. Dual energy CT (DECT), which has been used extensively in recent clinical trials, employs two X-ray energies. Based on the mass density of the material, the first X-ray spectrum distinguishes diverse elemental compositions with pixel values identical to those used in CT imaging. The second X-ray spectrum is used to do further attenuation measurements in order to categorize distinct tissue types and contrast agents. This allows for the determination of the mass density of two or three materials within a specified elemental composition combination. [4]

DECT has essentially supplanted conventional intravenous pyelography in urological stone diagnosis because it can properly determine the size and composition of urinary stones. It is critical to examine the stone's composition since UA stones can occasionally (less than 10% of the time) be eliminated after a lengthy metabolism and may be removed with medical therapy. Shockwave surgery or techniques used to remove urinary tract stones may cause kidney bleeding, fibrosis, and hypertension. If UA stones can be distinguished from non-UA stones, DECT testing may help some patients avoid unnecessary urinary tract treatment and its side effects. [5]

*Corresponding author: Magdi A. Ali *e-mail: magdi.ali@pua.edu.eg, Tel.: +2 1273917239
DOI: 10.21608/EJPHYSICS.2023.191799.1087
Received: 07/02/2023; Accepted: 13/04/2023

Material and Methods

CT equipment

Dual energy data set was acquired by (MDCT scanner (Aquilion 160-slice, Toshiba Medical Systems, Tokyo, Japan) using single-source dual-energy helical scan mode with a rapid switching system (rsDECT). Dual-energy helical scanning alternates between 80KVp, 460 mA and 135KVp, 80 mA. Fig. 1.

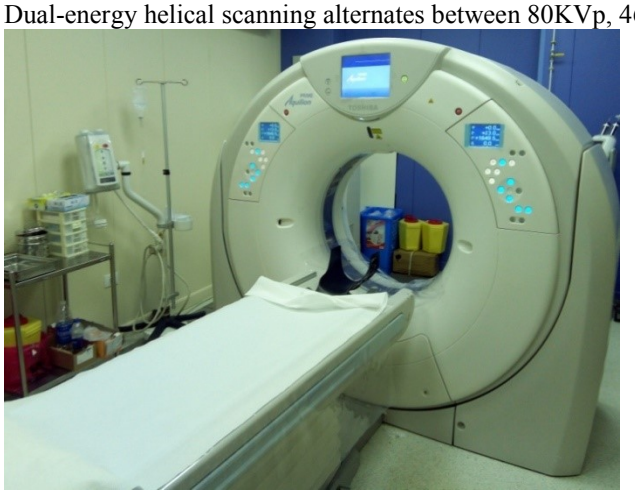

Fig.1. MDCT Aquilion Toshiba medical systems

Vitro study

Included are forty randomly collected urinary stones. Stones were available in different sizes, with a maximum transverse diameter of 33 mm and a minimum of 9 mm. Fig.2.

A cylindrical paraffin wax phantom was used in this study with a diameter of 10 cm and a carved cavity of bovine kidney shape. Fig.3,4.

Fresh bovine kidney models were used as phantoms. Fig.5.

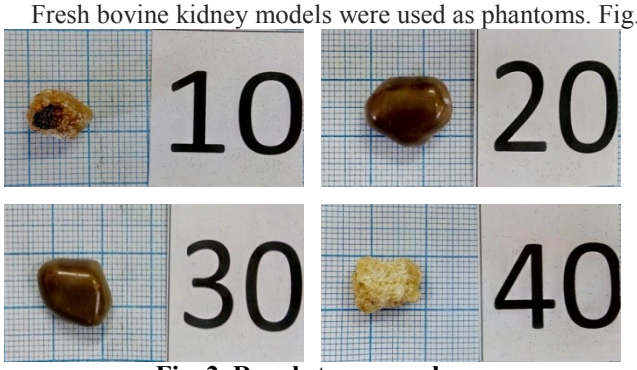

Fig. 2. Renal stone samples

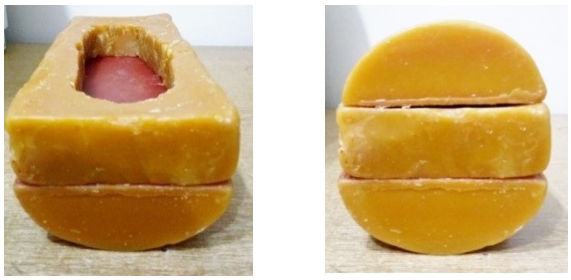

Fig.3. Paraffin Wax phantom

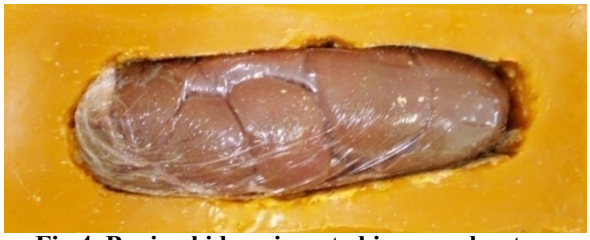

Fig.4. Bovine kidney inserted in wax phantom

Renal stone samples are placed in the bovine kidney pelvis and scanned using a single-source rapid switching DE technique with varying tube potentials. Then we repeated this scan after reinserting the bovine kidney containing stones into the wax phantom.

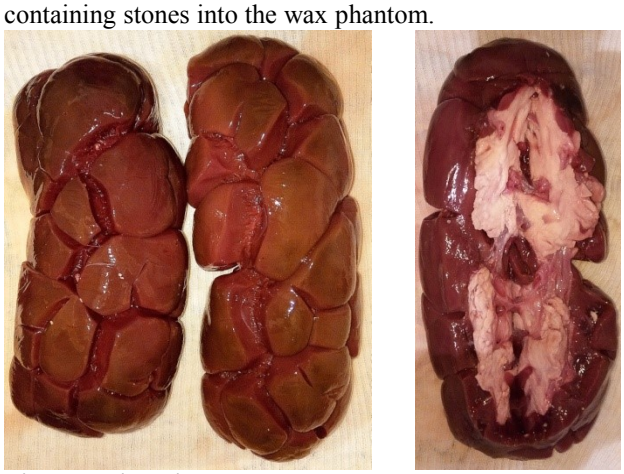

Fig.5. Bovine kidney model

The mean attenuation coefficient values (HU) measurements of the stones

A region of interest of (cm^2) was chosen for each stone based on the largest possible area through the stone's largest cross-sectional profile. Dataset assessment was performed with commercially available software applications (Syngo Multimodality Workplace, Siemens). The mean attenuation coefficient of each stone was measured in the DE images. [6] Dual Energy Ratio (DER):

DER was calculated by taking the ratio of mean attenuation at both KVp (HU80 and HU135) using the following equation.1. [7]

$$\text{DER} = \frac{\text{(HU)of stone measured at 80 kvp}}{\text{(HU)of the same stone measured at 135 kvp}} \quad (1)$$

Where HU means Mean attenuation coefficient of stone, 80 KVP, 135 KVP means scanning at low and high energy level.

Dual Energy Index (DEI):

Was calculated on a volumetric basis for stone characterization and measured using the following equation.2.

$$\text{DEI} = \frac{\text{DEN}}{\text{(HU)of stone at 80kvp+(HU) of same stone at 135kvp+2000)}} \quad (2)$$

Where DEN means dual energy number, HU means mean attenuation coefficient of stone, 80 KVP, 135 KVP means scanning at low and high energy level. [8]

Analysis of renal calculi by FTIR spectroscopy

After DE scanning, the renal stones are analyzed by FTIR. That was established in the analysis of urinary calculi composition. [9]

X-ray diffraction patterns

XRD is used to characterize and identify urinary calculi. It provides a well-organized, reliable facility, that can give clinicians reliable results. XRD was reported to be nearly 100% accurate, with no ambiguity in the analysis results. [10]

Results and Discussions

Characterization of Renal stones by DECT

HU of samples scanned in bovine kidney and after insertion in wax phantom: Fig.6. and Table 1, 2

(a) **(b)**

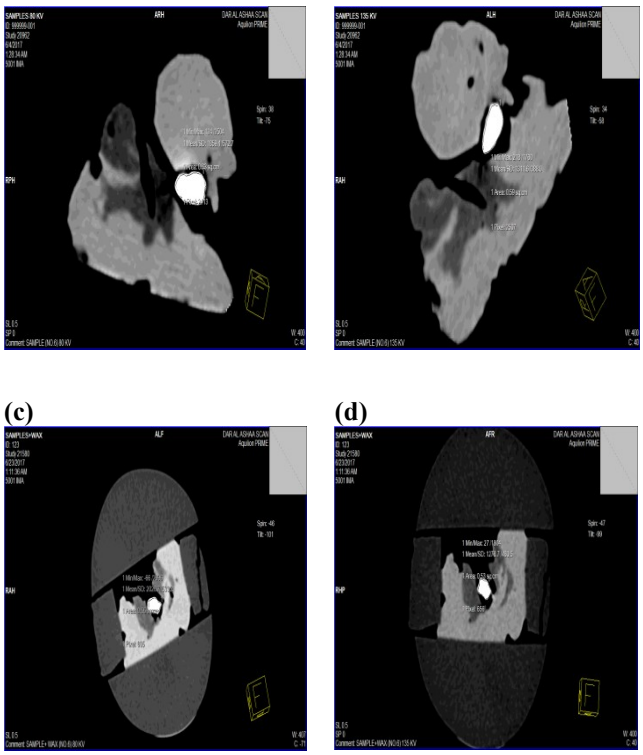

(c) **(d)**

Fig. 6. Sample No. 6 DECT Axial image measuring HU values in 80KV and 135KV as following:
(a) Scanned in bovine kidney in 80KV = 1859.4 HU.
(b) Scanned in bovine kidney in 135 KV = 1311.6 HU.
(c) Scanned in bovine kidney with wax phantom in 80 KV = 2026.7 HU.
(d) Scanned in bovine kidney with wax phantom in 135 KV = 1276.7 HU.

Attenuation coefficient measurements:

TABLE 1. HU of samples scanned in bovine kidney

Samples in bovine kidney and Wax	Mean HU value	
	80KV	135KV
1	2246.8	1686.4
2	1884.3	1276.7
3	1923.8	1254.6
4	1996.9	1310.3
5	1856.2	1240.2
6	2026.7	1276.7
7	1784.5	1217.3
8	1030.9	826.1
9	1104.2	802
10	1088.6	870.3
11	1851.9	1259.5
12	918.8	704.2
13	977.9	751.7
14	1602.4	1199.3
15	1722.9	1182.8
16	961.5	743.4
17	1067.3	860.2
18	1796.5	1174.6
19	1947.2	1225.4
20	1929.2	1191.2
21	1942	1175.7
22	1868.6	1151.4
23	1981	1253.3
24	2109.2	1331.6
25	1000.3	681.2
26	2002.2	1275.3
27	1868.6	1233.7
28	1037.5	739.1
29	1864	1273.1
30	1704.4	1149
31	1010.9	678.5
32	1719.8	1104.3
33	1112.2	751.7
34	1857.6	1227.1
35	1195.2	932.5
36	1723.9	1207.6
37	1006.1	760.9
38	237.1	229.5
39	211.6	207.4
40	1015.8	615.4

TABLE 2. HU of samples scanned in bovine kidney and wax

Samples in bovine kidney	Mean HU value	
	80KV	135KV
1	2198.9	1572.7
2	1835.5	1288.9
3	1689.7	1076.4
4	1869.1	1339.2
5	1742.2	1241.5
6	1859.4	1311.6
7	1593.4	1135.6
8	985.8	781.2
9	1013.2	765.1
10	1141.3	859.6
11	1716.7	1252.7
12	893.2	701
13	953.4	750.4
14	1599.7	1148.6
15	1678.8	1096.6
16	934.7	719
17	1006.4	747.4
18	1608.5	1142
19	1588.1	1119.3
20	1597.5	1124.8
21	1664.4	1194.2
22	1599.7	1168
23	1818.4	1356.8
24	1728.6	1325.1
25	913.7	681.9
26	1844.8	1391.6
27	1709.1	1239.9
28	929.1	716.2
29	1735.3	1260.2
30	1626.4	1116.1
31	883.9	663.5
32	1562.7	1049.2
33	1010.2	761.9
34	1663.3	1222.8
35	1334.2	960.4
36	1816.4	1432.7
37	921.9	731.8
38	240.5	218.9
39	265.2	236.2
40	830.3	657.5

Calculations:

Dual energy ratio (DER):

DER calculated for sample in bovine kidney Fig. 7, 8

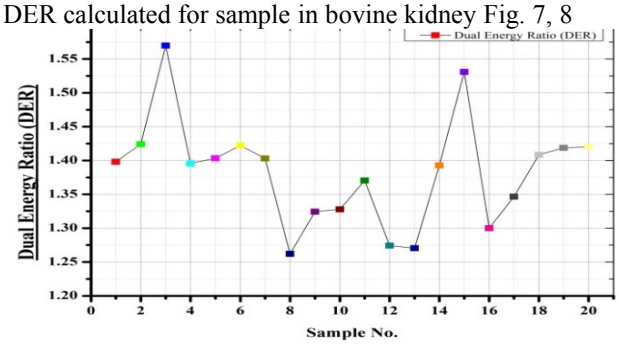

Fig. 7. DER for sample in bovine kidney from No.1 to No. 20

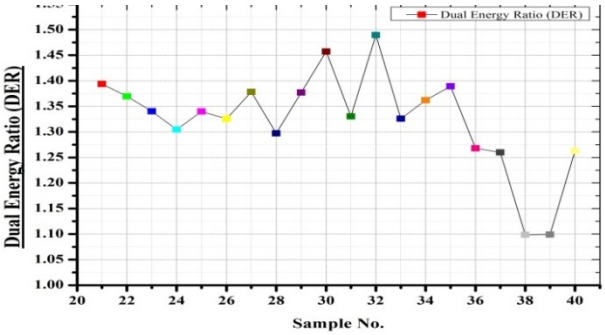

Fig. 8. DER for sample in bovine kidney from No.21 to No. 40

DER calculated for sample in bovine kidney within wax phantom Fig. 9, 10

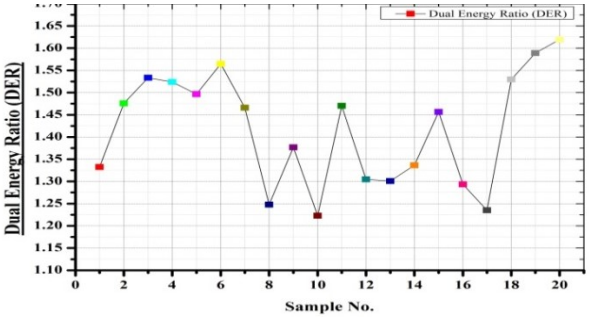

Fig. 9. DER for sample in bovine kidney within wax phantom from No.1 to No. 20

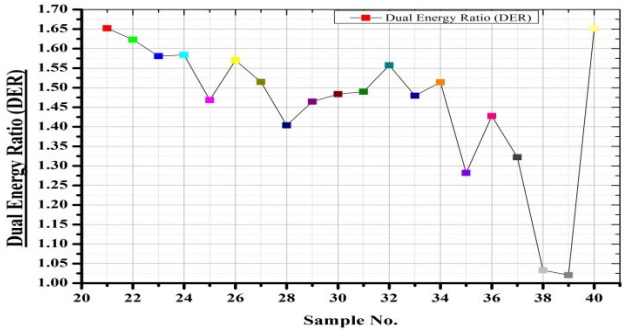

Fig.10. DER for sample in bovine kidney within wax phantom from No.21 to No. 40

The Dual Energy Index (DEI):

DEI calculated for sample in bovine kidney Fig.11,12.

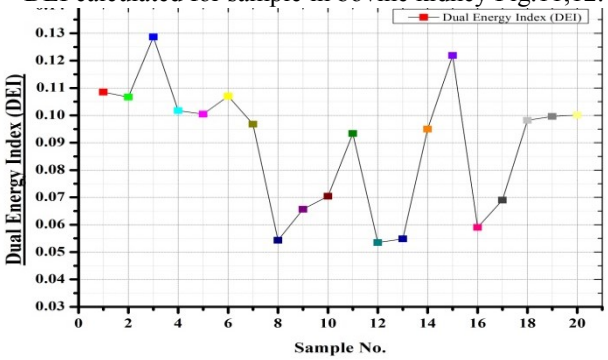

Fig.11.DEI for sample in bovine kidney from No.1 to No. 20

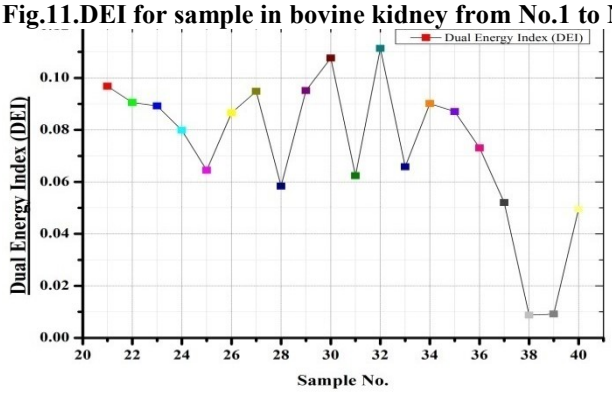

Fig.12. DEI for sample in bovine kidney from No.21 to No. 40

DEI calculated for sample in bovine kidney within wax phantom Fig. 13,14.

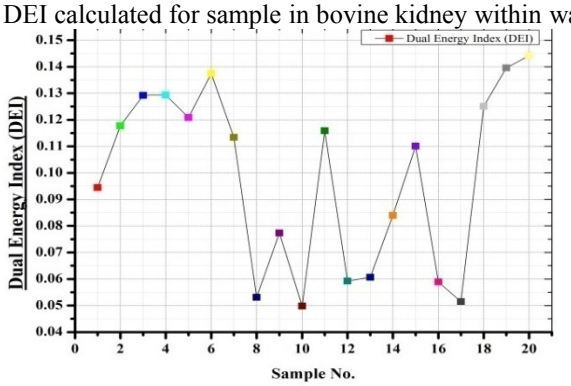

Fig. 13. DEI for sample in bovine kidney within wax phantom from No.1 to No. 20

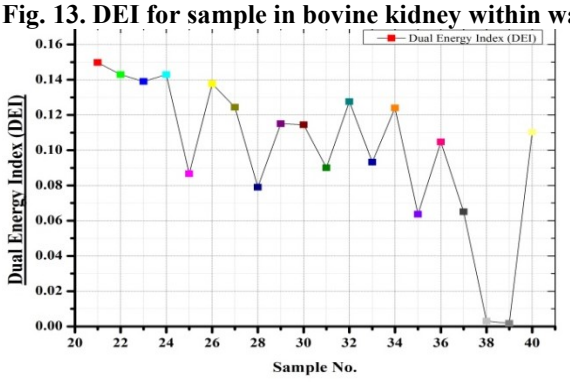

Fig. 14. DEI for sample in bovine kidney within wax phantom from No.21 to No. 40

Predicted stone type according to DER and DEI: (Table 3, 4)

Table 3. DECT scanning to the Samples in bovine kidney

Stones in bovine kidney	Predicted type according to	
	DER	DEI
1	Calcified	Calcified
2	Calcified	Calcified
3	Calcified	Calcified
4	Calcified	Calcified
5	Calcified	Calcified
6	Calcified	Calcified
7	Calcified	Calcified
8	Calcified	Calcified
9	Calcified	Calcified
10	Calcified	Calcified
11	Calcified	Calcified
12	Calcified	Calcified
13	Calcified	Calcified
14	Calcified	Calcified
15	Calcified	Calcified
16	Calcified	Calcified
17	Calcified	Calcified
18	Calcified	Calcified
19	Calcified	Calcified
20	Calcified	Calcified
21	Calcified	Calcified
22	Calcified	Calcified
23	Calcified	Calcified
24	Calcified	Calcified
25	Calcified	Calcified
26	Calcified	Calcified
27	Calcified	Calcified
28	Calcified	Calcified
29	Calcified	Calcified
30	Calcified	Calcified
31	Calcified	Calcified
32	Calcified	Calcified
33	Calcified	Calcified
34	Calcified	Calcified
35	Calcified	Calcified
36	Calcified	Calcified
37	Calcified	Calcified
38	UA	UA
39	UA	UA
40	Calcified	Calcified

TABLE 4. DECT scanning to the Samples in bovine kidney and wax phantom

Stones in bovine kidney and wax	Predicted type according to	
	DER	DEI
1	Calcified	Calcified
2	Calcified	Calcified
3	Calcified	Calcified
4	Calcified	Calcified
5	Calcified	Calcified
6	Calcified	Calcified
7	Calcified	Calcified
8	Calcified	Calcified
9	Calcified	Calcified
10	Calcified	Calcified
11	Calcified	Calcified
12	Calcified	Calcified
13	Calcified	Calcified
14	Calcified	Calcified
15	Calcified	Calcified
16	Calcified	Calcified
17	Calcified	Calcified
18	Calcified	Calcified
19	Calcified	Calcified
20	Calcified	Calcified
21	Calcified	Calcified
22	Calcified	Calcified
23	Calcified	Calcified
24	Calcified	Calcified
25	Calcified	Calcified
26	Calcified	Calcified
27	Calcified	Calcified
28	Calcified	Calcified
29	Calcified	Calcified
30	Calcified	Calcified
31	Calcified	Calcified
32	Calcified	Calcified
33	Calcified	Calcified
34	Calcified	Calcified
35	Calcified	Calcified
36	Calcified	Calcified
37	Calcified	Calcified
38	UA	UA
39	UA	UA
40	Calcified	Calcified

FTIR characterization of renal stones:

FTIR analysis for Sample No.1:

FTIR measurements of bands in the range 3477.85-3059.20 cm^{-1} could correspond to O–H or N–H, a weak band at 3059.20 cm^{-1}, a strong band around 1634.70 cm^{-1} could correspond to C=C stretching, two moderate intensity sharp bands at 1316.57 cm^{-1} could correspond to C-C symmetrical stretching and 780 cm^{-1} could correspond to C=O asymmetrical stretching, and three weak bands at 779.14, 659.73 and 514.69 cm^{-1}. These spectra indicate to calcium oxalate stone. Fig.15.

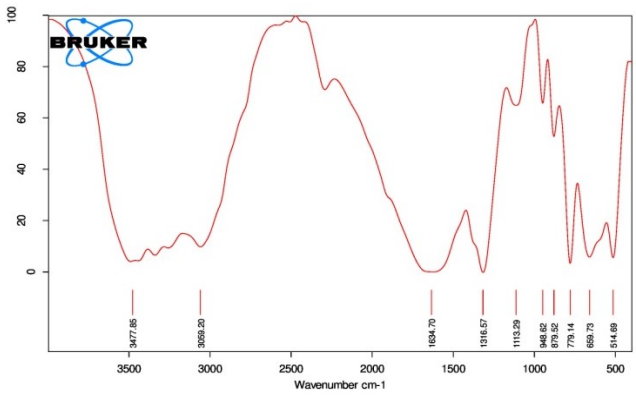

Fig. 15. Sample No.1 FTIR graph analysis

FTIR analysis Sample No.38:

FTIR measurements of the sample that presence of water and O-H stretching absorbed at 2933.51 cm^{-1}, a weak band at 3060.46 cm^{-1}, a strong band around 1637.71 cm^{-1} could correspond to C=O stretching, The band at 1120.18 cm^{-1}shows the ring vibration. N-H out-of- plane and in-plane bending observed at 873.87 cm^{-1}, The band at 782.61 cm^{-1} specifies skeletal ring deformation. These spectra indicate to UA stone. Fig. 16.

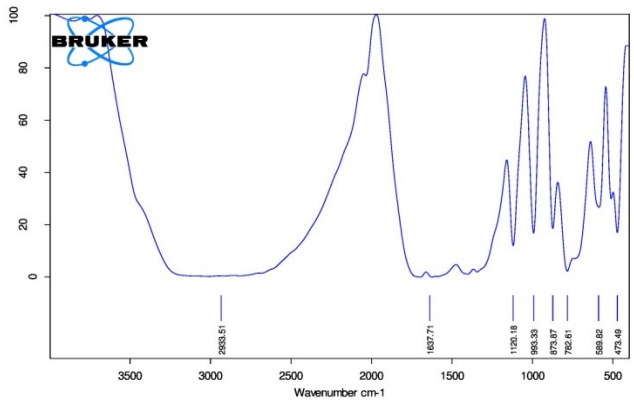

Fig. 16. Sample No.38 FTIR graph analysis

Renal stones characterization by XRD:

XRD spectrum analysis used to confirm renal stone composition.

XRD analysis Sample No.1:

XRD patterns of sample No. 1 exhibited the following diffraction peaks (2θ) at 24.4246, 38.1583 and 49.9714 which can be correlated to the (hkl) indices (200), (211), (213) of Calcium oxalate.Fig.17.

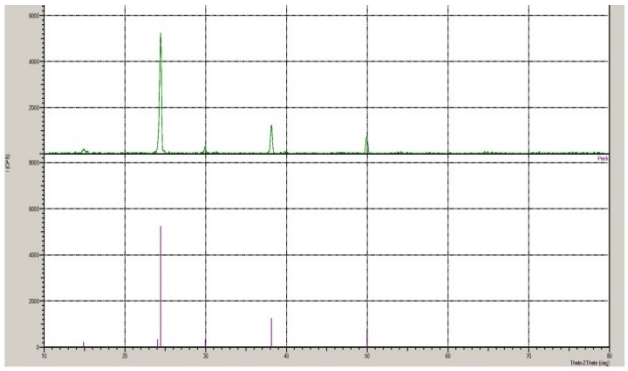

Fig. 17. Sample No.1 XRD graph analysis

XRD analysis Sample No.38:

XRD patterns of sample No. 38 exhibited the following diffraction peaks (2θ) at 28.56, 25.70 and 27.78 which can be correlated to the (hkl) indices (200), (211), (213) of UA. Fig. 18.

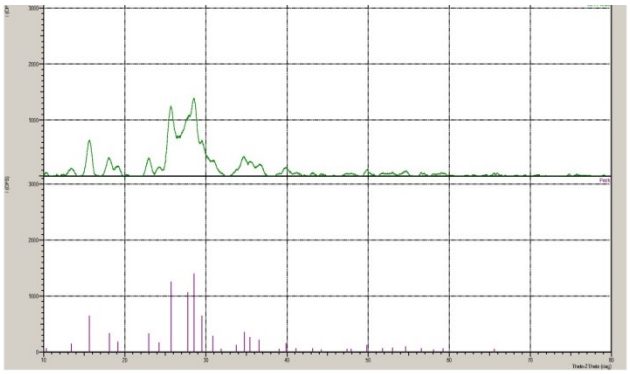

Fig. 18. Sample No.38 XRD graph analysis

Discussion

Stone composition is an important factor in determining appropriate medical management.[11]

In this study, mean linear attenuation coefficient which is the density per millimeter of an X-ray photon interaction depends on the X-ray energy used and average atomic number of stone samples. The DECT allows the differentiation of materials with low and high atomic numbers.

S. S. Bhawani. et al (2021). [9] categorized stones into four different groups using in vivo assessment: calcium oxalate, UA, cystine and hydroxyapatite stones according to DER ranged.

In the present study DER of all stones were found between 1.098-1.569 in samples scanned in bovine kidney, and between 1.020-1.651 in samples scanned in bovine kidney within wax phantom. 38/40 (95%) stones assessed have DER greater than 1.24 that indicate calcium stones and 2/40 (5%) have DER less than 1.1that indicate UA stones.

Rescanning renal stone samples in bovine kidney within wax phantom showed 38/40 (95%) having DER greater than 1.24 that indicate calcium stones and 2/40 (5%) have DER less than 1.1that indicate UA stones.

In the present study DER of less than 1.1 indicated of UA stone and ratios greater than 1.24 indicated calcified stone. These results totally agreed with the study S. S. Bhawani. et al. [9]

In the present study DEI of the renal stone samples from attenuation coefficient at high and low energies levels were calculated. The DEI was found between 0.008-0.129 in Samples scanned in bovine kidney and between 0.002-0.144 in Samples scanned in bovine kidney within wax phantom.

Samples scanned in bovine kidney model found 38/40 stone (95%) having DEI higher than 0.0413 and 2/40 stone (5%) have DEI less than 0.0269.

B. Yadav and S. Maharjan (2017) [12]. Dual energy ratios were ranged from 0.55-1.11 for UA stone, 1.12-1.24 for cystine and more than 1.24 for calcium oxalate and hydroxyapatite stones. The mean HU noted in our study were; for UA stones (461.12 ± 119 HU at 80 kV, 449 ± 98.5 HU at 140 kV), for cystine (870.79 ± 386 at 80 kV, 743 ± 341 at 140 kV), for calcium oxalate (1246 ± 448 at 80 kV, 915 ± 316 at 140 kV) for hydroxyapatite

(1301 ± 387 at 80 kV, 896 ± 315 at 140 kV) and mixed stone had (779.25 ± 269 HU at 80 kV, 665.5 ± 252 HU at 140 kV).

Rescanning the same renal stone samples in bovine kidney after insertion in wax phantom found 38/40 stone (95%) having DEI higher than 0.0413 and 2/40 stone (5%) of DEI less than 0.0269.

In the present study DEI found between 0.0071-0.0269 indicates to UA stones and DEI higher than 0.0413 indicates to calcium stones.

A. Primiano et al (2014). [13] recommends the use of FTIR for urinary stone analysis.

In the present study, four renal stones sample (two samples UA stones and two samples calcium stones as been detected by DECT) were analyzed using FTIR and results compared with DECT. We observed calcium stones in 2/4 samples (50%) and UA stones in 2/4 samples (50%) using the FTIR. The percentage was matching with DECT results and reached 100%.

A. Ali. et al (2022). [14] stated that there is no doubt that XRD is the most appropriate method to determine mineral structures. XRD can distinguish all the different crystal types in a particular mixture.

N. Arita-Merino et al (2020). [15] stated that XRD has advantages of reliability in qualitative analysis and accuracy in quantitative analysis.

In the present study, four renal stone (two UA stones and the other two calcium stones as a detected in result from DECT) were analyzed using XRD method. Based on the search match analysis performed on the Powder XRD data using standard database, constituents of four stones have been identified. Renal stones were identified using XRD, and their elemental composition was interrogated through using of XRD database. We observed calcium stones in 2/4 samples (50%) and UA stones in 2/4 samples (50%) using the XRD method. The percentage of matching with DECT results reached to (100%).

Conclusion

DECT is not only used in the diagnosis of urinary system stones concerning their location and size but can also be used to determine the renal stones' composition.

The volume of perinephric fat surrounding the kidney, which does not affect and contributes to the chemical composition of DECT renal stone characterization, is considered ineffective in the characterization of renal stones when using a wax phantom in DECT scanning.

DECT in this in-vitro study could possibly replace the standard CT methods used in the diagnosis of urolithiasis due to their high accuracy in classifying renal stone compositions.

Our in-vitro results showed that using linear attenuation coefficient values, DER and DEI, unenhanced DECT at both energies levels of 80 kV and 135 kV is a credible method for differentiating UA and calcium-containing calculi. DECT can provide a rapid and noninvasive examination to diagnose presence, size, location and determination the composition of renal stones.

References

1. L. Yue, Q. Pai, X. Wu, and J. Zhang, “Smoking and Risk of Urolithiasis: Meta-Analysis of Observational Studies,” *Front. Public Heal.*, vol. 10, no. March, pp. 1–7, 2022.
2. S. Saghamanesh, H. Richter, A. Neels, and R. Zboray, “Multi-Modal X-ray Imaging and Analysis for Characterization of Urinary Stones,” *Appl. Sci.*, vol. 12, no. 8, 2022.
3. J. Y. Jeong, K. S. Cho, D. H. Kim, D. Y. Jun, Y. J. Moon, and J. Y. Lee, “A New Parameter for Calcium Oxalate Stones : Impact of Linear Calculus Density on Non-Contrast Computed Tomography,” *Medicina (B. Aires).*, vol. 59, no. 267, pp. 1–12, 2023.
4. B. Mussmann, M. Hardy, H. Jung, M. Ding, P. J. Osther, and O. Graumann, “Can Dual Energy CT with Fast kV-Switching Determine Renal Stone Composition Accurately?,” *Acad. Radiol.*, vol. 28, no. 3, pp. 333–338, 2021.
5. M. Stępień, R. Chrzan, and W. Gawlas, “In vitro analysis of urinary stone composition in dual-energy computed tomography,” *Polish J. Radiol.*, vol. 83, pp. e421–e425, 2018.
6. S. Khanduri *et al.*, “Role of Dual Energy CT Scan in Evaluation of the Chemical Composition of Renal Stones,” *J. Clin. Diagnostic Res.*, vol. 14(6), no. 1–4, pp. 4–7, 2020.
7. G. S. K. Fung *et al.*, “Differentiation of kidney stones using dual-energy CT with and without a tin filter,” *Am. J. Roentgenol.*, vol. 198, no. 6, pp. 1380–1386, 2012.

8. A. Graser *et al.*, "Dual energy CT characterization of urinary calculi: Initial in vitro and clinical experience," *Invest. Radiol.*, vol. 43, no. 2, pp. 112–119, 2008.
9. S. S. Bhawani, M. Jehangir, M. Masood, S. A. Dar, and S. N. Syed, "Dual-Energy Multidetector Computed Tomography: A Highly Accurate Non-Invasive Tool for in Vivo Determination of Chemical Composition of Renal Calculi," *Galician Med. J.*, vol. 28, no. 3, p. E202134, 2021.
10. M. Gadelmoula *et al.*, "Can stone composition be predicted by plain X-ray and/or non-contrast CT? A study validated by X-ray diffraction analysis," *African J. Urol.*, vol. 26, no. 1, 2020.
11. S. Shalini, V. K. Arunachalam, R. K. Varatharajaperumal, P. Mehta, S. Thambidurai, and M. Cherian, "The role of third-generation dual-source dual-energy computed tomography in characterizing the composition of renal stones with infrared spectroscopy as the reference standard," *Polish J. Radiol.*, vol. 87, no. 1, pp. e172–e176, 2022.
12. B. Yadav and S. Maharjan, "Characterization of Urinary Tract Stones with Dual Energy Computed Tomography," *Radiogr. Open*, vol. 3, no. 1, p. 11, 2017.
13. A. Primiano *et al.*, "FT-IR analysis of urinary stones: a helpful tool for clinician comparison with the chemical spot test," *Dis. Markers*, vol. 2014, p. 176165, 2014.
14. A. Ali, Y. W. Chiang, and R. M. Santos, "X-Ray Diffraction Techniques for Mineral Characterization: A Review for Engineers of the Fundamentals, Applications, and Research Directions," *Minerals*, vol. 12, no. 2, 2022.
15. N. Arita-Merino, H. Van Valenberg, E. P. Gilbert, and E. Scholten, "Quantitative Phase Analysis of Complex Fats during Crystallization," *Cryst. Growth Des.*, vol. 20, no. 8, pp. 5193–5202, 2020.